



UDC 620.19

STUDY OF THE PHOSPHATE ADHESION ON STAINLESS STEEL SURFACES: INVESTIGATION OF CLOGGING AND GEOGRAPHICAL SETTINGS

Mustapha Adar^{1*}, Mohcine Chakouri², Majda Medkour¹, Zakarya Abbassi³, Youssef Najih¹,
Jamaa Bengourram¹, Mustapha Mabrouki¹

¹Industrial Engineering Laboratory, Sultan Moulay Slimane University, Faculty of Science and Technology, PO Box 523, Beni Mellal, Morocco.

²Team of Remote Sensing and GIS Applied to the Geosciences and the Environment, Faculty of Sciences and Technology, Beni Mellal 23000, Morocco

³Laboratory of Search in Physics and Science for Engineer, Polydisciplinary Faculty, Sultan Moulay Slimane University, Beni Mellal, Morocco

Received 24 March 2024; accepted 10 October 2024; available online 15 April 2025

Abstract

Clogging, a physicochemical adhesion phenomenon, occurs between material surfaces, prompting our investigation into phosphate adhesion on steel surfaces and its associated clogging. Phosphate pellets, produced under varying pressures (80–340 bars) with 25 % water content, were analyzed after drying at 60 °C. Physicochemical interactions were explored through contact angle measurements, showing a decrease from 71° to 65° as compaction pressure increased, and surface energy calculations indicated an increase from 49 mJ/m² to 52.5 mJ/m². The phosphate originated from the extraction zone of the OCP in Ben Guerir, Morocco. Contact angle measurements on stainless steels (304, 304L, and 316) revealed that 316 steel exhibited hydrophobic behavior (contact angle 94°, surface energy 35 mJ/m²), while 304 and 304L were hydrophilic with contact angles of 68° and 70°, and surface energies of 48 mJ/m² and 45 mJ/m², respectively. Atomic force microscopy (AFM) revealed that 316 steel had the highest roughness (Ra = 45 nm) compared to 304 and 304L (Ra = 32 nm and 34 nm). A predictive adhesion model showed that 316 steel promotes phosphate adhesion (negative free energy of adhesion), while 304 and 304L steels displayed positive free energies, indicating weaker adhesion. These findings provide key parameters for understanding phosphate fouling on solid supports.

Keywords: adhesion; AFM; clogging; phosphate; standard stainless steels; surface energy.

ДОСЛІДЖЕННЯ АДГЕЗІЇ ФОСФАТІВ НА ПОВЕРХНЯХ З НЕРЖАВІЮЧОЇ СТАЛІ: ДОСЛІДЖЕННЯ ЗАБРУДНЕНЬ ТА ГЕОГРАФІЧНИХ УМОВ

Мустафа Адар¹, Мохсіне Чакурі², Маджда Медкур¹, Закарія Аббассі³, Юсеф Наджіх¹,
Джамаа Бенгуррам¹, Мустафа Мабрукі¹

¹Лабораторія промислового інжинірингу. Університет Султана Мулая Слімана, факультет науки і технологій, а/с 523, Бені Меллал, Марокко.

²Група дистанційного зондування і ГІС у застосуванні до наук про Землю і навколишнє середовище, Науково-технічний факультет, Бені Меллал, 23000, Марокко

³Лабораторія пошуку у фізиці та науці для інженерів, Міждисциплінарний факультет, Університет Султана Мулая Слімана, Бені Меллал, Марокко

Анотація

Між поверхнями матеріалів відбувається забруднення за рахунок явища фізико-хімічної адгезії, що спонукало нас дослідити адгезію фосфатів на сталевих поверхнях і пов'язане з нею забруднення. Фосфатні гранули, виготовлені під різними тисками (80–340 бар) з 25 %-ним вмістом води, були проаналізовані після сушіння за 60 °C. Фізико-хімічні взаємодії були досліджені шляхом вимірювання кута розтікання, який зменшився з 71° до 65° зі збільшенням тиску ущільнення, а розрахована поверхнева енергія збільшилась з 49 мДж/м² до 52.5 мДж/м². Фосфат походить із зони видобутку в Бен-Герірі, Марокко. Вимірювання кута розтікання на нержавіючих сталях (304, 304L і 316) показало, що сталь 316 має гідрофобну поведінку (кут розтікання 94°, поверхнева енергія 35 мДж/м²), а сталі 304 і 304L виявилися гідрофільними, з кутами розтікання 68° і 70° і поверхневими енергіями 48 мДж/м² і 45 мДж/м² відповідно. Атомно-силова мікроскопія показала, що сталь 316 має найвищу шорсткість (Ra = 45 нм) порівняно з 304 і 304L (Ra = 32 нм і 34 нм). Модельювання адгезії показало, що сталь 316 сприяє адгезії фосфатів (негативна вільна енергія адгезії), а 304 і 304L мають позитивну вільну енергію, що свідчить про слабшу адгезію. Ці результати надають ключові параметри для розуміння фосфатних відкладень на твердих опорах.

Ключові слова: адгезія; АСМ; забруднення; фосфати; стандартні нержавіючі сталі; поверхнева енергія.

*Corresponding author: e-mail: adar.mustapha@gmail.com

Introduction

Morocco presently stands as a key contributor to global phosphate production, constituting 20 % of the world's output and ranking as the second-largest producer following the United States. Moreover, it leads as the primary exporter, commanding 45 % of the global market. The transportation of extracted phosphate to hoppers via large-capacity trucks, however, is marred by the persistent challenge of fouling and clogging on truck bodies, resulting in substantial economic ramifications. The elucidation of the clogging mechanism and the underlying interactions governing phosphate adhesion to tippers becomes imperative.

The phenomenon of clogging, engendering material adhesion, emanates from the system's innate proclivity to mitigate surface energy. Consequently, adhesion manifests as a process characterized by adhesion work, denoting adhesion strength. The reversibility of this adhesion mechanism remains nontrivial, particularly due to possible reactions between interacting materials in direct contact [1–5]. Numerous factors intricately influence material adhesion, prominently including intrinsic surface characteristics such as surface morphology [6], roughness [7–9], grain size and crystallinity [10], chemical constituents at the surface [11; 12]. Among these characteristics, wettability, hydrophobicity and surface energy are of primary importance [13–20], which have a direct impact on adhesion mechanisms [21], consequently impacting mechanical clogging and inking [22; 23].

This study is principally dedicated to comprehending the phosphate clogging phenomenon on standard steels employed in industrial contexts, specifically in trucks' tippers for raw phosphate transportation. The primary objective is to furnish a physicochemical characterization by measuring the contact angle and calculating the surface energy of phosphates in pellet form and stainless steels. Additionally, a topographic characterization and roughness measurement via atomic force microscopy are conducted to visualize the steel support topography. Furthermore, an analytical model is employed to scrutinize phosphate adhesion, providing insights into the phenomenon of

phosphate clogging on steels. Notably, the findings underscore that the physicochemical properties of the steel supports exert a discernible influence on the initiation of clogging.

Experimental methods

Geographical and stratigraphical settings

From a geographical standpoint, the study area is located within the municipality of Oulad Hassoune Hamri, situated in the Gantour basin, at the heart of the Benguerir region which is located between Casablanca and Marrakech in the center of Moroccan territory. Stratigraphically, this region is renowned for its phosphate formations, which have been the subject of numerous studies since 1965. These formations, ranging from the Upper Cretaceous to the Eocene, primarily consist of silica and carbonate [24–26].

Regarding the different stratigraphic layers:

The Maastrichtian phosphate begins with a coarse texture and concludes with a silico-marginal complex. It is divided into two distinct terms, separated by a layer of yellow clay known as the Maastrichtian, which plays a key role in the Gantour basin.

The Danian typically starts with a limestone phosphate and ends with a silico-marginal complex, containing the most significant phosphate layer in the series. The Thanetian is characterized by an extensive layer of sand-phosphate, covered by marls. The Ypresian consists of a marl-siliceous complex accompanied by a phosphate furrow. The Lutetian marks the end of the phosphate formation process and is distinguished by a slab of dolomitic limestone containing thersitae.

Fig. 1 provides a general overview of the geographical location of the study area.

Preparation of steel samples

Stainless steel, recognized for its robust mechanical attributes and superior corrosion resistance, stands as a versatile alloy extensively employed across diverse sectors including mechanical engineering, food processing, chemical industries, and transportation [27]. This section outlines a physicochemical investigation involving three distinct types of stainless steel—304, 304L, and 316. The substrates of each steel coupon (2×2 cm) underwent a preliminary cleansing process with distilled water.

VAN OSS [30]. Thomas Young defined the contact angle (θ) of a liquid drop on an ideal and planar solid surface in mechanical equilibrium by considering the interplay of three interfacial tensions:

$$\gamma_{SV} = \gamma_{SL} + \gamma_{LV} \cos \theta \quad (1)$$

Here γ_{LV} , γ_{SV} , and γ_{SL} represent the liquid-vapor, solid-vapor, and solid-liquid interfacial tensions, respectively, and θ is the contact angle.

Van Oss' model incorporates the acid-base approach, which accounts for molecular interactions through electron donor/acceptor processes, considering complementary properties of the liquid and solid. The total surface energy (γ) is expressed as the sum of Lifshitz-Van der Waals (LW) forces (γ^{LW}) and acid-base interactions (γ^{AB}):

$$\gamma = \gamma^{LW} + \gamma^{AB} \quad (2)$$

For the calculation of the surface energy, a minimum of three liquids is required: one non-polar liquid and two polar liquids following the Lewis scale [31]. Therefore, the surface energy equation can be written as follows:

$$(\cos \theta + 1)/2 = (\gamma_s^{LW} \gamma_L^{LW})^{1/2} / \gamma_L + (\gamma_s^+ \gamma_L^-)^{1/2} / \gamma_L + (\gamma_s^- \gamma_L^+)^{1/2} / \gamma_L \quad (3)$$

Here, θ represents the measured contact angle, γ^{LW} is the Van der Waals free energy component, γ^+ is the electron acceptor component, and γ^- is the electron donor component. According to Van Oss, Chaudhury and Good [32], water is considered the reference solvent, and the surface energy component values for the utilized liquids are detailed in Table 1.

Table 1.

| Liquid | Surface Energy Components (mJ/m ²) | | | | |
|------------------|--|-----------------|-----------------|--------------|--------------|
| | γ_L | γ_L^{LW} | γ_L^{AB} | γ_L^+ | γ_L^- |
| Water | 72.8 | 21.8 | 51.0 | 25.5 | 25.5 |
| Formamide | 58.0 | 39.0 | 19.0 | 2.28 | 39.6 |
| Methylene iodide | 50.8 | 50.8 | ≈ 0 | ≈ 0 | ≈ 0 |

c) Quantitative hydrophobicity

The quantitative hydrophobicity of a given material (i), denoted as the variation of the total free energy, is defined as the change in the free energy of interaction between two interfaces of $\Delta G_{iwi} = -2[(\gamma_i^{LW})^{1/2} - (\gamma_i^{LW})^{1/2}]^2 + 2[(\gamma_i^+ \gamma_i^-)^{1/2} - (\gamma_w^+ \gamma_w^-)^{1/2} - (\gamma_i^+ \gamma_w^-)^{1/2} - (\gamma_w^+ \gamma_i^-)^{1/2}]$ (4)

A negative value of ΔG_{iwi} indicates an attractive free energy of interaction between molecules, signifying a hydrophobic character of the solid surface—implying that the surface has less affinity for water than among its own components. Conversely, when $\Delta G_{iwi} > 0$, the solid surface is deemed hydrophilic, signifying a greater affinity for water.

d) Theoretical model of adhesion prediction: thermodynamic approach

In accordance with the thermodynamic approach [32], the adhesion energy ΔG_{adh} , also referred to as Gibbs free energy, exerted by a particle undergoing a transition from a system with two interfaces (particle/liquid (γ_{pl}), liquid/substrate (γ_{sl})) to a system with one interface (particle/substrate (γ_{ps})), corresponds to the free energy variation of the system. The

the material immersed in water (W) [28]. This metric comprises two components: acid-base (AB) and dispersive (LW). The equation expressing the free energy of interaction is delineated as follows:

thermodynamic approach is mathematically expressed through the following equation:

$$\Delta G_{adh} = \gamma_{ps} - \gamma_{pl} - \gamma_{sl} \quad (5)$$

This physicochemical approach represents a comprehensive framework for elucidating particle attachment on surfaces, taking into consideration diverse attractive and repulsive interactions such as Van der Waals, electrostatic, or dipolar forces, collectively expressed in terms of free energy. Successful application of this approach necessitates the numerical estimation of thermodynamic parameters, including particle surface free energy and substrate surface free energy, to calculate the Gibbs adhesion energy.

Adhesion is energetically favored only when ΔG_{adh} is negative. The adhesion free energy ΔG_{pls} can be decomposed into two distinct components: the Lifshitz van der Waals (ΔG_{pls}^{LW}) and acid-base (ΔG_{pls}^{AB}) components:

$$\Delta G_{pls} = \Delta G_{pls}^{LW} + \Delta G_{pls}^{AB}, \quad (6)$$

where:

$$\Delta G_{pls}^{LW} = ((\gamma_p^{LW})^{1/2} - (\gamma_s^{LW})^{1/2})^2 - ((\gamma_p^{LW})^{1/2} - (\gamma_l^{LW})^{1/2})^2 - ((\gamma_s^{LW})^{1/2} - (\gamma_l^{LW})^{1/2})^2 \quad (7)$$

$$\Delta G_{pls}^{AB} = 2[(\gamma_l^+)^{1/2} [(\gamma_p^-)^{1/2} + (\gamma_s^-)^{1/2} - (\gamma_l^-)^{1/2}] + (\gamma_l^-)^{1/2} [(\gamma_p^+)^{1/2} + (\gamma_s^+)^{1/2} - (\gamma_l^+)^{1/2}] - ((\gamma_p^+ \gamma_s^-)^{1/2} \times (\gamma_p^- \gamma_s^+)^{1/2})] \quad (8)$$

Results and discussion

Physicochemical characterization of phosphate

The physicochemical analysis of phosphate was carried out by measuring the contact angle

and calculating the surface energy on pellets of phosphate, as shown in Fig. 2, compacted under various pressures.



Fig. 2. Phosphate pellets obtained under the following pressures: 80, 100, 140, 200, 240, 300 and 340 bars

To perform contact angle measurements on the phosphate pellets, we first identify the equilibrium time of the solvent drop used in this study. For this reason, we perform kinetics of the

water contact angle on the surface of the phosphate pellet as well as the volume of the drop as depicted in Fig. 3.

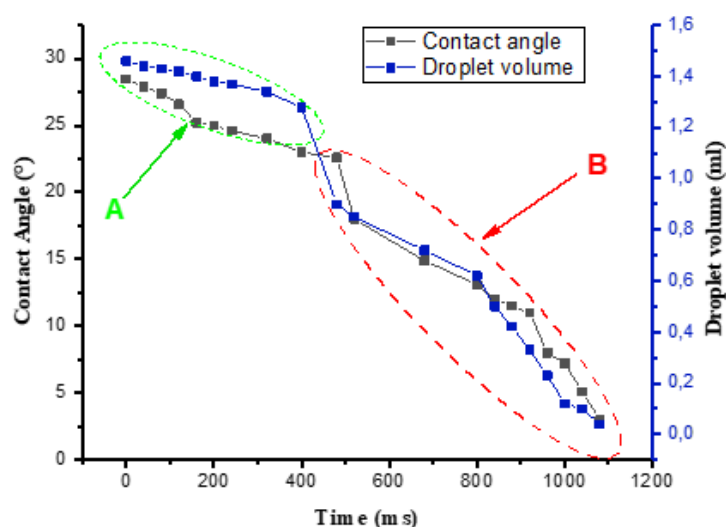


Fig. 3. Kinetics of the contact angle and the droplet volume on the pellet

In region (A), the contact angle of the water decreases slowly on the surface of the phosphate pellet, this is the phase of the drop equilibrium. In region (B), the values of the contact angle and the drop volume decrease quickly as a function of time. This is the phase of the liquid absorption on the phosphate surface. This can be explained by

the high value of the phosphate surface energy. The obtained results (contact angle values, surface energy components and hydrophobicity) of the different pellets under various pressures (80, 100, 140, 200, 240, 300 and 340 bar) are grouped in table 2.

Table 2

Contact angle values and surface energy components of the phosphate pellets

| Phosphate pellets | Contact angle (°) | | | Surface Energy components (mJ/m ²) | | | | | ΔG_{iwi} (mJ/m ²) |
|-------------------|-------------------|------------|------------|--|------------|------------|---------------|----------------|---------------------------------------|
| | θ_w | θ_F | θ_D | γ^{LW} | γ^+ | γ^- | γ^{AB} | γ^{Tot} | |
| P ₈₀ | 29.00 | 33.20 | 21.30 | 47.39 | 0.01 | 52.65 | 1.56 | 48.96 | 33.80 |
| P ₁₀₀ | 26.90 | 30.90 | 24.40 | 46.37 | 0.00 | 53.04 | 0.85 | 47.21 | 35.43 |
| P ₁₄₀ | 22.90 | 30.00 | 22.20 | 47.11 | 0.00 | 56.62 | 0.25 | 47.36 | 40.19 |
| P ₂₀₀ | 20.10 | 22.30 | 18.40 | 48.24 | 0.05 | 53.83 | 3.22 | 51.46 | 33.82 |

| | | | | | | | | | |
|------------------|-------|-------|-------|-------|------|-------|------|-------|-------|
| P ₂₄₀ | 21.70 | 23.30 | 18.00 | 48.35 | 0.04 | 53.06 | 2.82 | 51.16 | 32.97 |
| P ₃₀₀ | 16.60 | 20.10 | 14.50 | 48.97 | 0.04 | 55.35 | 3.07 | 52.04 | 35.45 |
| P ₃₄₀ | 16.80 | 19.30 | 15.10 | 49.06 | 0.05 | 54.79 | 3.42 | 52.48 | 34.43 |

From Table 2, we observe that the compacting pressure of the phosphate pellets slightly increased the surface energy. For a pressure of 80 bars, the value of the surface energy is about 49 mJ/m². While for a maximum pressure of 340 bars the value of the surface energy is equal to 52.5 mJ/m². Therefore, the variation of the pressure caused a modification of the interactions at the interface of the phosphate pellets.

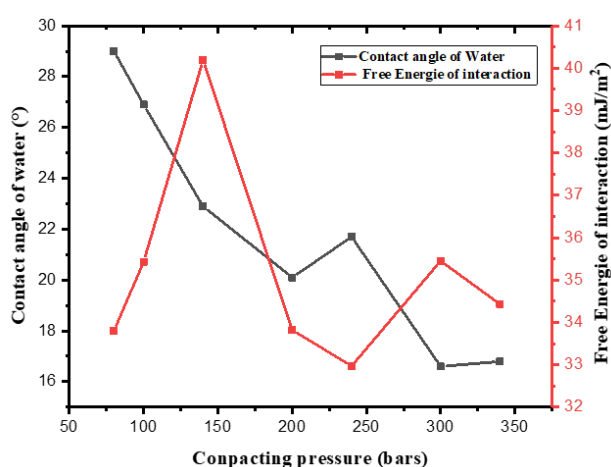


Fig. 4. Variation of the contact angle of water and hydrophobicity

Fig. 4 shows the evolution of the contact angle as a function of the compacting pressure. We can see that as the pressure increases the contact angle of the water drop decreases. This result shows that the pressure has changed the physicochemical properties of the pellet surface, i.e., the topographical structure has changed as a function of pressure, such as roughness and porosity. We can also see from Fig. 4 that the surfaces of the various pellets are hydrophilic (ΔG_{iwi} is positive). The pellet obtained at 140 bar has the highest value of free energy of interaction.

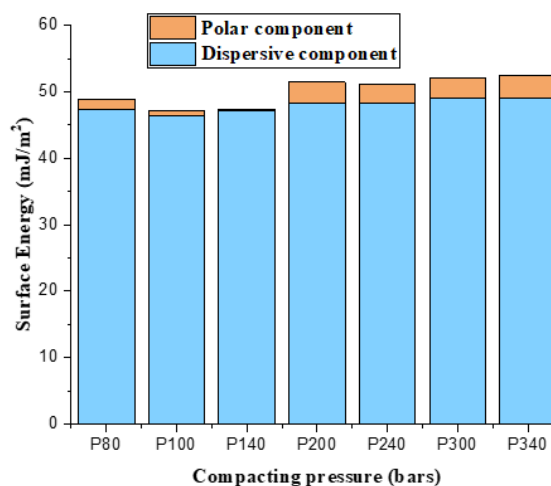


Fig. 5. Surface energy components of phosphate pellets

In addition, Fig. 5 shows the influence of compacting pressure on the surface energy components. We find that the pellets obtained under different pressures have a fairly large dispersive component compared to the polar component. It has been shown that the pellet surfaces are governed by long-range intermolecular forces. Analyzing the electron acceptor/donor character by decomposing the polar (acid-base) component into an acid component and a base component, we find that the base component has the highest value in all pellets. Then, the surfaces of these pellets have a very important electron acceptor character as presented in the results of Table 2.

Physicochemical characterization of steel supports

The hydrophobic/hydrophilic properties, surface energy components and acid-base properties of stainless-steel support surfaces were evaluated using contact angle measurements.

Table 3

Contact angle values and surface energy components of stainless-steel supports

| Steel supports | Contact angle (°) | | | Surface Energy components (mJ/m ²) | | | | | ΔG_{iwi} (mJ/m ²) |
|----------------|-------------------|------------|------------|--|------------|------------|---------------|----------------|---------------------------------------|
| | θ_w | θ_F | θ_D | γ^{LW} | γ^+ | γ^- | γ^{AB} | γ^{Tot} | |
| 304 | 23.07 | 33.70 | 44.60 | 37.24 | 0.31 | 58.46 | 8.45 | 45.68 | 42.60 |
| 304L | 54.23 | 46.03 | 43.10 | 38.03 | 0.18 | 28.16 | 4.42 | 42.45 | -1.42 |
| 316 | 80.67 | 52.47 | 26.93 | 45.44 | 0.08 | 3.50 | 1.05 | 46.48 | -69.38 |

The calculation of the surface energy and its components was performed using the Van Oss

approach, the results are presented in Table 3. All three supports have a very large dispersive

component of surface energy compared to the polar component. On the other hand, 316 steel has a very low value of the polar component of surface energy. This result is already proven by the

calculation of the free energy of interaction. By analyzing the hydrophobic/hydrophilic character, steel 304 is hydrophilic (ΔG_{iwi} is positive) while 304L and 316 are hydrophobic (ΔG_{iwi} is negative).

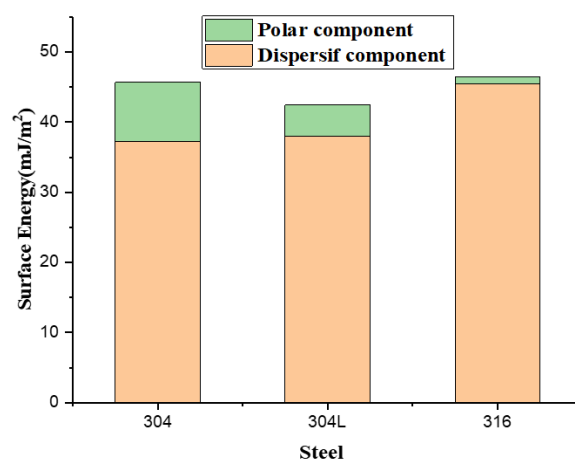


Fig. 6. Surface energy components of steel supports (304, 304L, 316)

Fig. 6 shows the fraction of each component of surface energy relative to total energy. We observe that the surfaces of the various samples are governed by the Lifshitz-Van Der Waals long-range forces. We also find from the acid-base properties that all steel supports have a strong electron acceptor character.

Topographic characterization of steel supports using AFM

The topographies of the samples used in this study are characterized by atomic force microscopy. The images obtained from the three steel supports (304, 304L and 316) are shown in Figs. 7, 8 and 9. Compared to a 2D surface roughness meter, the AFM not only measures the surface roughness, but also displays a 3D image showing the surface morphology of the measured area and indicating possible defects at the micro and nano scale

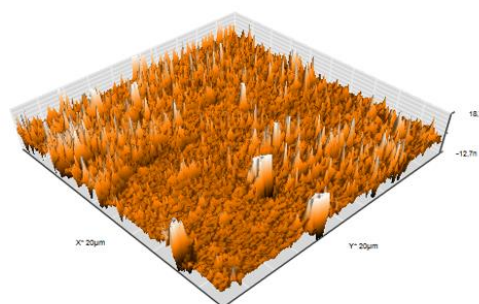
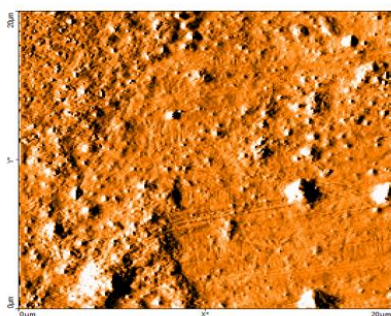


Fig. 7. AFM images of 304 steel (2D and 3D)

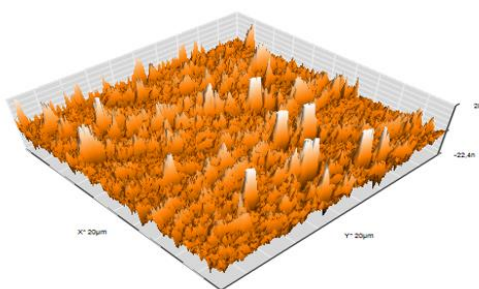
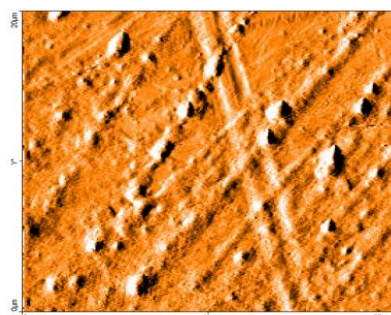


Fig. 8. AFM images of 304L steel (2D and 3D)

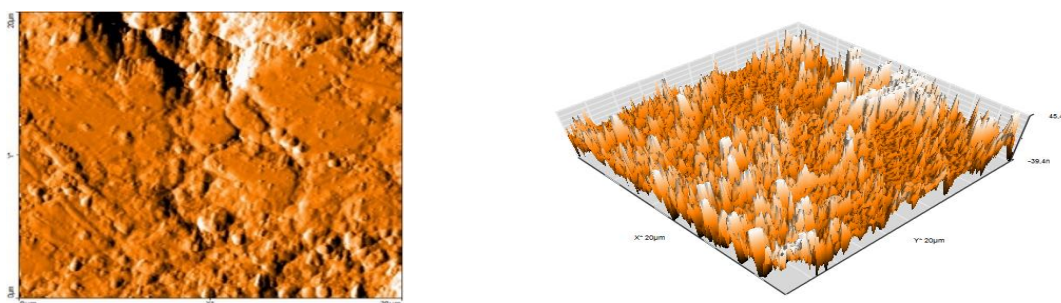


Fig. 9. AFM images of 316 steel (2D and 3D)

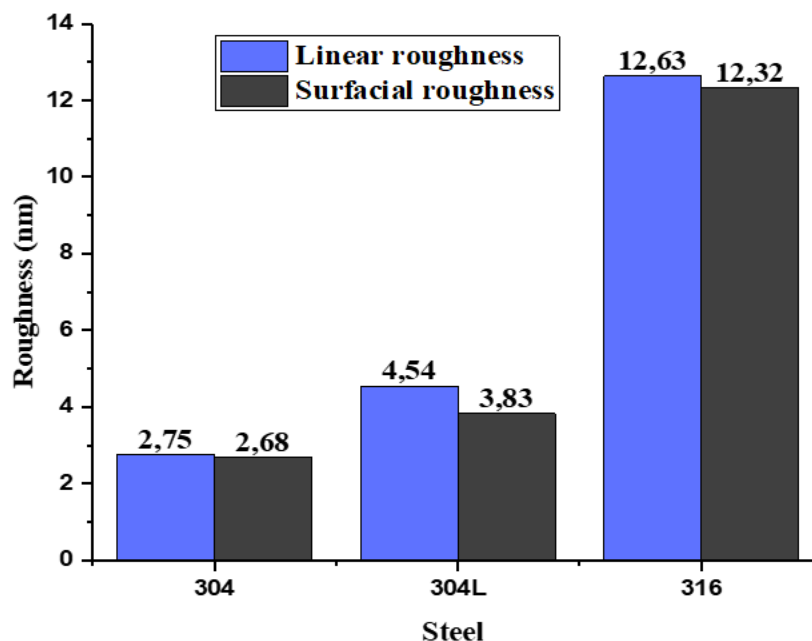


Fig. 10. Linear and surface roughness of steel (304, 304L and 316)

From the images obtained, we observe that each steel surface has a different topography. This result is evaluated by calculating the roughness of each steel. Using advanced image analysis by the Esayscan 2 software of the Nanosurf Flex AFM device, the surface properties of different substrates can be described by a set of roughness parameters. A selected number of roughness parameters calculated for the samples are shown in Fig. 10. We note that 316 steel has the highest value of linear and surface roughness. The other supports have almost the same roughness values. It can be said here that the roughness typically changes the physicochemical properties of the steel. This provides this support with a hydrophilic aspect and a very important electron acceptor character.

Prediction of phosphate adhesion on stainless steels

In the first part, we calculated the surface energies of both phosphate pellets and stainless steels using the contact angle technique. We extracted all the physicochemical parameters in order to exploit it in this section to establish a

predictive study of the adhesion of phosphate on the surface of steels which we will assimilate as the first stage of clogging. By the thermodynamic approach we have calculated the free energy of adhesion of the pellet-steel system to predict the primary adhesion of the phosphate particles.

The adhesion prediction study was carried out on steels (304, 304L and 316) and phosphate pellets that were compacted at variable pressures (80, 100, 140, 200, 240, 300 and 340 bars).

Fig. 11 summarizes the results of the prediction of the phosphate adhesion on steel supports. For 304 and 304L steels, the values of adhesion energy calculated by the thermodynamic approach are positive. Following these values, it can be confirmed theoretically that the adhesion is not favored. In contrast to 316 steel, the values of adhesion energy calculated on its surface are negative, i.e. the adhesion of phosphate on 316 steel is favored. This diversity of the calculated adhesion energy values of the different steel-pellets systems is explained by the physicochemical and topographical properties. 316 steel has a higher roughness than 304 and

304L steel. Concerning the physicochemical properties, the substrates of 304 and 304L steel have a very strong electron-donor character, which disadvantages the creation of chemical bonds between phosphate and steel. Furthermore, we observe that the pressure does not have a significant influence on the adhesion energy. The phosphate pellets obtained under pressure $P = 140$ bar always have the highest value of the adhesion energy. According to Fig. 11, we can see that 304 and 304L steel has a repulsive aspect (yellow region), while 316 steel has an attractive aspect (blue regions) because of the base component of the surface energy and also because of the negative value of the free energy interaction (hydrophobicity).

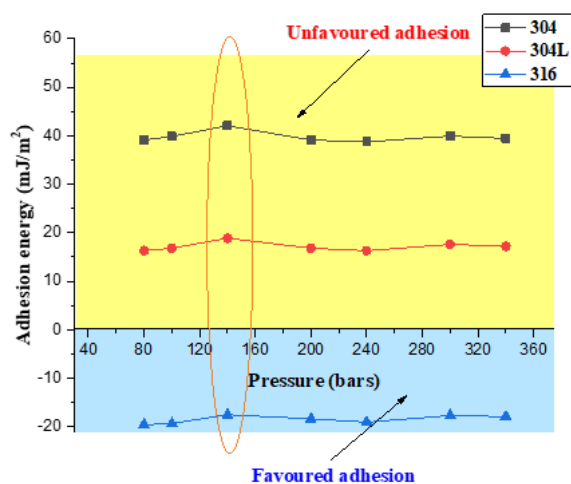


Fig. 11. Adhesion energy of steel-pellets systems

The adhesion of phosphate on stainless steel surfaces is governed by a combination of chemical interactions and surface properties. Chemically, phosphate adhesion is driven by electrostatic attractions, hydrogen bonding, and in some cases, covalent bonding. Phosphates can form coordination complexes with metal cations on the surface of stainless steel, particularly with oxides such as iron, chromium, and nickel present in the steel's passive layer. These interactions are influenced by the surface energy of both materials, where the phosphate's electron donor character plays a critical role in bonding with the electron-

acceptor components of the steel's surface energy. The adhesion is further influenced by the roughness and composition of the stainless steel surface. Increased surface roughness, as observed with 316 steel, enhances mechanical interlocking and provides more surface area for chemical interactions, which favors phosphate adhesion. In contrast, smoother surfaces, such as those of 304 and 304L steel, exhibit lower phosphate adhesion due to reduced roughness and a stronger electron-donor character that impedes the formation of chemical bonds with phosphate. Surface treatments, such as polishing or passivation, can further modify the oxide layer's thickness and composition, affecting the adhesion process by altering the surface energy and the interaction potential between phosphate and stainless steel. The combination of these factors—chemical bonding mechanisms and surface properties like roughness and composition—collectively determines the efficiency and strength of phosphate adhesion on stainless steel surfaces.

Conclusion

The work carried out in this paper focuses on determining the parameters that affect the clogging and phosphate adhesion on steels. A physicochemical study was performed in order to analyze the interactions involved in the phenomenon of phosphate clogging. Based on the surface energy calculation of phosphate pellets, we found that the surface of phosphate has a hydrophilic character and is governed by long-range forces (larger dispersive components in front of the polar component). 304 and 304L steels have hydrophilic character, and 316 steel has hydrophobic character. Moreover, topographic parameters and roughness calculated from atomic force microscopy of steels showed that 316 steel has the highest value of arithmetic roughness. By studying the prediction of phosphate adhesion to steels, we found that adhesion favors 316 steel, which presents an attractive aspect opposite to the other steels (304 and 304L).

References

- [1] Webster, J., Tricard, M. (2004). Innovations in abrasive products for precision grinding, *CIRP Ann. - Manuf. Technol.*, 53(2), 597–617, 2004, doi: [10.1016/S0007-8506\(07\)60031-6](https://doi.org/10.1016/S0007-8506(07)60031-6).
- [2] Brinksmeier, E., Mutlugünes, Y., Klocke, F., Aurich, J. C., Shore, P., Ohmori, H. (2010). Ultra-precision grinding," *CIRP Ann.*, 59(2), 652–671. doi: [10.1016/j.cirp.2010.05.001](https://doi.org/10.1016/j.cirp.2010.05.001).
- [3] Badger, J., Murphy, S., O'Donnell, G. E. (2010). Loading in Grinding: Chemical Reactions in Steels and Stainless Steels," *Adv. Mater. Res.*, 126–128, 597–602. doi: [10.4028/www.scientific.net/AMR.126-128.597](https://doi.org/10.4028/www.scientific.net/AMR.126-128.597).
- [4] Patnaik Durgumahanti, U. S., Singh, V., Venkateswara Rao, P. (2010). A New Model for Grinding Force Prediction and Analysis, *Int. J. Mach. Tools Manuf.*, 50(3), 231–240, doi: [10.1016/j.ijmachtools.2009.12.004](https://doi.org/10.1016/j.ijmachtools.2009.12.004).
- [5] Najih, Y., Adar, M., Medkour, M., Bengourram, J., Mabrouki, M. (2023). The Effect of Roughness on the Physicochemical Properties of a36 Steel: Phosphate Adhesion Study, *J. Chem. Technol.*, 31(3), 581–589, doi: [10.1016/j.jct.2023.03.001](https://doi.org/10.1016/j.jct.2023.03.001).

- [10.15421/jchemtech.v3i1i3.278149](https://doi.org/10.15421/jchemtech.v3i1i3.278149).
- [6] Costa, D. O. (2013). The differential regulation of osteoblast and osteoclast activity by surface topography of hydroxyapatite coatings, *Biomaterials*, 34(30), 7215–7226. doi: [10.1016/j.biomaterials.2013.06.014](https://doi.org/10.1016/j.biomaterials.2013.06.014).
- [7] Advincula, M.C., Rahemtulla, F.G., Advincula, R. C., Ada, E.T., Lemons, J. E., Bellis, S. L. (2006). Osteoblast adhesion and matrix mineralization on sol-gel-derived titanium oxide., *Biomaterials*, 27(10), 2201–2212, doi: [10.1016/j.biomaterials.2005.11.014](https://doi.org/10.1016/j.biomaterials.2005.11.014).
- [8] Lampin, M., Warocquier-Clérout, C., Legris, M., Degrange, Sigot-Luizard, M. F. (1997). Correlation between substratum roughness and wettability, cell adhesion, and cell migration., *J. Biomed. Mater. Res.*, 36(1), 99–108, doi: [10.1002/\(sici\)1097-4636\(199707\)36:1<99::aid-jbm12>3.0.co;2-e](https://doi.org/10.1002/(sici)1097-4636(199707)36:1<99::aid-jbm12>3.0.co;2-e).
- [9] Rouahi, M., Champion, E., Hardouin, P., Anselme, K. (2006). Quantitative kinetic analysis of gene expression during human osteoblastic adhesion on orthopaedic materials, *Biomaterials*, 27(14), 2829–2844 doi: [10.1016/j.biomaterials.2006.01.001](https://doi.org/10.1016/j.biomaterials.2006.01.001).
- [10] Dasgupta, S., Tarafder, S., Bandyopadhyay, A., Bose, S. (2013). Effect of grain size on mechanical, surface and biological properties of microwave sintered hydroxyapatite., *Mater. Sci. Eng. C. Mater. Biol. Appl.*, 33(5), 2846–2854, doi: [10.1016/j.msec.2013.03.004](https://doi.org/10.1016/j.msec.2013.03.004).
- [11] Y. Wang, S. Zhang, X. Zeng, L. L. Ma, K. A. Khor, and M. Qian, "Initial attachment of osteoblastic cells onto sol-gel derived fluoridated hydroxyapatite coatings," *J. Biomed. Mater. Res. Part A*, vol. 84A, no. 3, pp. 769–776, 2008, <https://doi.org/10.1002/jbm.a.31289>.
- [12] Yang, L., Perez-Amodio, S., Barrère-de Groot, F. Y. F., Everts, V., van Blitterswijk, C. A., Habibovic, P. (2010). The effects of inorganic additives to calcium phosphate on in vitro behavior of osteoblasts and osteoclasts," *Biomaterials*, 31(11), 2976–2989, doi: [10.1016/j.biomaterials.2010.01.002](https://doi.org/10.1016/j.biomaterials.2010.01.002).
- [13] Autumn, K., Gravish, N. (2008). Gecko adhesion: evolutionary nanotechnology, *Philos. Trans. R. Soc. A Math. Phys. Eng. Sci.*, 366(1870), 1575–1590, 2008, doi: [10.1098/rsta.2007.2173](https://doi.org/10.1098/rsta.2007.2173).
- [14] Wang, L., Zhou, Q. (2014). Nepenthes pitchers: surface structure, physical property, anti-attachment function and potential application in mechanical controlling plague locust, *Chinese Sci. Bull.*, 59(21), 2513–2523, doi: <https://doi.org/10.1007/s11434-014-0383-6>.
- [15] Feng L. (2002). Super-Hydrophobic Surfaces: From Natural to Artificial, *Adv. Mater.*, 14(24), 1857–1860, doi: <https://doi.org/10.1002/adma.200290020>.
- [16] Guo, Z., Liu, W., Su, B.-L. (2011). Superhydrophobic surfaces: from natural to biomimetic to functional., *J. Colloid Interface Sci.*, 353(2), 335–355, doi: [10.1016/j.jcis.2010.08.047](https://doi.org/10.1016/j.jcis.2010.08.047).
- [17] Bhushan, B. (2009). Biomimetics: lessons from nature—an overview, *Philos. Trans. R. Soc. A Math. Phys. Eng. Sci.*, 367(1893), 1445–1486, doi: [10.1098/rsta.2009.0011](https://doi.org/10.1098/rsta.2009.0011).
- [18] Elyaagoubi, M., Najih, Y., Khadiri, M., Mabrouki, M., Oueriagli, A., Outzourhit, A. (2017). Electrochemically deposited Bismuth-Telluride nanowires in nanoporous alumina, *Membranes*, 8, 2070–2075.
- [19] Najih, Y., Adar, M., Charafih, Y., Rahmani, K., Khaouch, Z., Mabrouki, M. (2019). Elaboration and characterization of zno thin films structural and optical study, *J. Phys. Conf. Ser.*, 1292(1), doi: [10.1088/1742-6596/1292/1/012009](https://doi.org/10.1088/1742-6596/1292/1/012009).
- [20] Adar, M., Najih, Y., Charafih, Y., Rahmani, K., Khaouch, Z., Mabrouki, M. (2019). Elaboration and characterization of zno thin films structural and optical study," in *Journal of Physics: Conference Series*, doi: [10.1088/1742-6596/1292/1/012009](https://doi.org/10.1088/1742-6596/1292/1/012009).
- [21] Jeandin, M., Koivuluoto, H., Vezzu, S. (2015). Coating Properties BT - Modern Cold Spray: Materials, Process, and Applications, J. Villafuerte, Ed., *Cham: Springer International Publishing*, 107–224. doi: [10.1007/978-3-319-16772-5_4](https://doi.org/10.1007/978-3-319-16772-5_4).
- [22] Wu, S. (1982). *Polymer interface and adhesion*. New York SE - Marcel Dekker New York. doi: [LK - https://worldcat.org/title/807302380](https://doi.org/10.1007/978-1-4613-0238-0).
- [23] Weiss, H. (1995). Adhesion of advanced overlay coatings: mechanisms and quantitative assessment, *Surf. Coatings Technol.*, 71(2), 201–207, doi: [10.1016/0257-8972\(94\)01022-B](https://doi.org/10.1016/0257-8972(94)01022-B).
- [24] Anjjar, A., Driouch, Y., Benjelloun, F., Hmeid, H. A., El Alami, A. (2020). The phosphate series of Benguerir (Maastrichtian-Ypresian, Morocco): Mineralogy and mine planning, *J. Mater. Environ. Sci.*, 2020(4), 574–583.
- [25] Henri C. (2014). Marine vertebrate faunas from the Maastrichtian phosphates of Benguerir (Ganntour Basin, Morocco): Biostratigraphy, palaeobiogeography and palaeoecology, *Palaeogeogr. Palaeoclimatol. Palaeoecol.*, 409. doi: [10.1016/j.palaeo.2014.04.020](https://doi.org/10.1016/j.palaeo.2014.04.020).
- [26] Daafi, Y., Chakir, A., Jourani, E., Ouabba, S. M. (2014). Geology and Mine Planning of Phosphate Deposits: Benguerir Deposit Gantour Basin - Morocco, *Procedia Eng.*, 83, 70–75, doi: [10.1016/j.proeng.2014.09.014](https://doi.org/10.1016/j.proeng.2014.09.014).
- [27] Hamadi F., Latrache, H. (2008). Comparison of contact angle measurement and microbial adhesion to solvents for assaying electron donor–electron acceptor (acid–base) properties of bacterial surface, *Colloids Surfaces B Biointerfaces*, 65(1), 134–139. doi: [10.1016/j.colsurfb.2008.03.010](https://doi.org/10.1016/j.colsurfb.2008.03.010).
- [28] Os, V. (2006). *Interfacial Forces in Aqueous Media (2nd ed.)*. New York: CRC press. doi: <https://doi.org/10.1201/9781420015768>.
- [29] Young, T. (1805). III. An essay on the cohesion of fluids," *Philos. Trans. R. Soc. London*, 95, 65–87. doi: [10.1098/rstl.1805.0005](https://doi.org/10.1098/rstl.1805.0005).
- [30] Van Oss, C.-J., Good, R.-J., Chaudhury, M.-K. (1986). The role of van der Waals forces and hydrogen bonds in "hydrophobic interactions" between biopolymers and low energy surfaces, *J. Colloid Interface Sci.*, 111(2), 378–390, doi: [10.1016/0021-9797\(86\)90041-X](https://doi.org/10.1016/0021-9797(86)90041-X).
- [31] Van Oss, C. J., Chaudhury, M. K., Good, R. J. (1986). Monopolar surfaces, *Adv. Colloid Interface Sci.*, 28(C), 35–64, doi: [10.1016/0001-8686\(87\)80008-8](https://doi.org/10.1016/0001-8686(87)80008-8).
- [32] Morra M., Cassinelli, C. (1997). Bacterial adhesion to polymer surfaces: a critical review of surface thermodynamic approaches., *J. Biomater. Sci. Polym. Ed.*, 9(1), 55–74, doi: [10.1163/156856297x00263](https://doi.org/10.1163/156856297x00263).